IOPscience iopscience.iop.org

Home Search Collections Journals About Contact us My IOPscience

Modeling cytoskeletal flow over adhesion sites: competition between stochastic bond dynamics and intracellular relaxation

This article has been downloaded from IOPscience. Please scroll down to see the full text article.

2010 J. Phys.: Condens. Matter 22 194112

(http://iopscience.iop.org/0953-8984/22/19/194112)

View the table of contents for this issue, or go to the journal homepage for more

Download details:
IP Address: 129.252.86.83
The article was downloaded on 30/05/2010 at 08:03

Please note that terms and conditions apply.

IOP Publishing Journal of Physics: Condensed Matter

J. Phys.: Condens. Matter **22** (2010) 194112 (10pp) doi:10.1088/0953-8984/22/19/194112

Modeling cytoskeletal flow over adhesion sites: competition between stochastic bond dynamics and intracellular relaxation

Benedikt Sabass[1,2] **and Ulrich S Schwarz**[1,3]

[1] Bioquant, University of Heidelberg, Im Neuenheimer Feld 267, 69120 Heidelberg, Germany
[2] II. Institute for Theoretical Physics, University of Stuttgart, 70550 Stuttgart, Germany
[3] Institute for Theoretical Physics, University of Heidelberg, Philosophenweg 19, 69120 Heidelberg, Germany

E-mail: Ulrich.Schwarz@bioquant.uni-heidelberg.de

Received 9 November 2009, in final form 24 January 2010
Published 26 April 2010
Online at stacks.iop.org/JPhysCM/22/194112

Abstract

In migrating cells, retrograde flow of the actin cytoskeleton is related to traction at adhesion sites located at the base of the lamellipodium. The coupling between the moving cytoskeleton and the stationary adhesions is mediated by the continuous association and dissociation of molecular bonds. We introduce a simple model for the competition between the stochastic dynamics of elastic bonds at the moving interface and relaxation within the moving actin cytoskeleton represented by an internal viscous friction coefficient. Using exact stochastic simulations and an analytical mean field theory, we show that the stochastic bond dynamics lead to biphasic friction laws as observed experimentally. At low internal dissipation, stochastic bond dynamics lead to a regime of irregular stick-and-slip motion. High internal dissipation effectively suppresses cooperative effects among bonds and hence stabilizes the adhesion.

(Some figures in this article are in colour only in the electronic version)

1. Introduction

Migration and adhesion of tissue cells relies on the continuous formation and dissociation of adhesion sites based on transmembrane receptors from the integrin-family (so-called focal adhesions, FAs) [1, 2]. FAs provide a mechanical link between the actin cytoskeleton and the extracellular environment and in addition act as signaling centers [3]. In mature cell adhesion, they are mainly coupled to actin bundles (so-called stress fibers), which are contracted by myosin II motors. In cell migration, they are mainly coupled to the retrograde flow of the actin mesh, which is driven not only by myosin II contractility close to the cell body, but also by actin polymerization at the leading edge. In all cases, the actin cytoskeleton and the focal adhesions are very dynamic, with all components being in a state of continuous flow [4, 5]. However, the details of how flow in the actin cytoskeleton is coupled to the dynamics of protein localization and force transmission at focal adhesions are not clear.

In experiments with migratory cells, actin motion can be identified as the drift of fluorescent speckles in the actin mesh over the FAs. For different cell types, including growth cones and keratocytes, it has been found that the slower the retrograde flow, the faster the cell protrusion, suggesting that the growing actin network pushes the cell envelope forward if sufficiently stalled at the FAs [6–9]. These findings have led to the suggestion that FAs can act as molecular clutches: as the clutch engages, retrograde flow slows down and protrusion is increased [10, 11]. A possible molecular basis are adapter proteins like talin, α-actinin and vinculin involved in the binding between the integrin receptors and the actin cytoskeleton. Indeed, it has been found that the constituents of FAs move with different speeds, with a low speed for the integrins, an intermediate speed for vinculin and a high speed for actin [12, 13].

Correlation of actin speed with traction recently became possible by combining fluorescent speckle microscopy with traction force microscopy [14]. The new method was used to construct spatial maps of traction and intracellular actin flow in migratory epithelial cells. Maxima of traction were observed where adhesion proteins clustered, predominantly a few micrometers behind the leading edge of the cell. Actin

 © 2010 IOP Publishing Ltd Printed in the UK & the USA

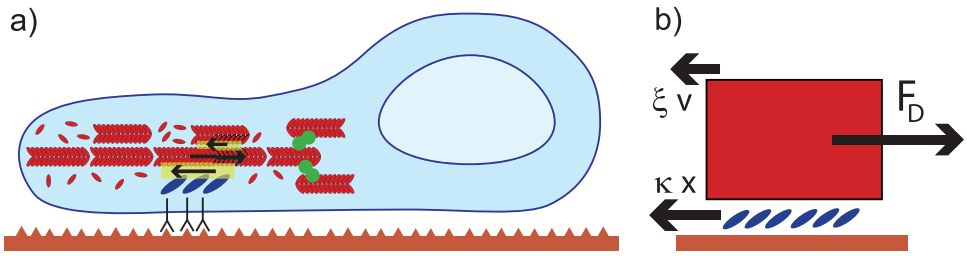

Figure 1. Schematics of the situation of interest. (a) Biological system: the retrograde flow of actin (red) from left to right is caused by polymerization pushing at the front and by myosin motors (green) pulling at the back. It is slowed down at sites of adhesion composed of layers of adhesion receptors (black) and adapter molecules (blue). The transparent yellow boxes mark the two main regions of dissipation which correspond to two forces counteracting the flow: stochastic dynamics of elastic bonds at the adhesion sites (bottom box) and viscous dissipation in the cytoskeleton (top box), e.g. due to sliding friction between neighboring filaments. (b) Model: the driving force for sliding (F_D, right arrow) is balanced by time-varying elastic forces at the interface (κx, bottom left arrow) and velocity-dependent viscous forces inside the cell (ξv, top left arrow).

speed, on the other hand, was maximal at the very edge of the cell. Analysis of the data revealed that the dependence of traction on actin speed followed a robust biphasic relationship where force transmission was maximal at an intermediate actin speed of around 10 nm s^{-1}. These findings suggest that rate-dependent processes are essential for the regulation of FAs, in particular for their clutch function.

The physical understanding of friction at moving interfaces is a long standing and still very active research field [15]. It has been shown early by Schallamach that modeling of friction by discrete microscopic bonds can lead to biphasic behavior in the velocity–stress relation [16]. Recently this has been confirmed by more elaborate computer simulations [17] and analytical calculations [18]. Another important and often observed feature of these systems is stick–slip behavior, which typically occurs at intermediate velocities. This body of work in the field of tribology demonstrates that the interplay between movement, binding and force creates a rich phenomenology of interesting effects. However, the consequence of this for the way cells sense and react to their environment have hardly been explored, although the underlying molecular mechanisms show some intriguing similarities. A notable exception is a recent experimental–theoretical study on the dynamic retraction of filopodia on compliant substrates [19]. However, because this treatment included many details of the particular system of interest (including a force–velocity-relation for retraction by myosin molecular motors), it is not sufficiently generic to be easily transferred to similar situations of interest. In another recent study on clutch dynamics, a kinetic model has been introduced to study the turnover rates of the different proteins involved [20]. Although very successful in explaining experimental data [12, 13], this kinetic approach does not address issues of spatial coordination and force transmission.

Here we introduce a simple model which allows us to study the generic aspects of molecular bonding at moving interfaces. We apply our approach to study theoretically how force is transmitted from the flowing actin cytoskeleton through the FAs to the substrate, where it has been measured before as a traction force. Instead of confronting the full complexity of the cellular system, we focus on one particular aspect, namely the competition between the stochastic dynamics of elastic bonds at the moving interface and additional modes of relaxation within the actin cytoskeleton. As common in this field, we model the bonds as harmonic springs which are elongated by the moving interface once they are bound. However, it is important to note that the binding dynamics at the moving interface is not the only source of dissipation. In practice the flowing actin gel is a plastic–viscoelastic body which features many additional modes of dissipation, including the rupture of crosslinks inside the actin cytoskeleton and the dissipative contributions from the hydrolysis cycles of the molecular motors. The simplest way to model this situation is to lump all these additional processes into one effective internal viscous friction coefficient. In the force balance, the elastic contributions from the bonds at the interface are thus complemented by an internal dissipative force. From the mechanical point of view, we deal with a Kelvin–Voigt model in which the elastic part obeys some stochastic dynamics.

We find that our simple model can lead to a surprisingly rich behavior which allows us to draw interesting conclusions regarding the experimental results. The relation between average force and average speed for such a system is highly non-linear and shows a maximum of transmitted force for intermediate speeds, as observed experimentally [14] and as expected from earlier theoretical work [16–18]. We analyze the dependence of this relation on model parameters such as the number of bonds and internal viscous friction. Internal friction, damping the movement of the actin, is found to play an important role in suppressing rupture cascades and thus in stabilizing the adhesions. We demonstrate the existence of an unsteady stick–slip-motion for low internal viscous friction at intermediate driving forces. The existence of this regime poses an important constraint on the operation of regulatory mechanisms acting at adhesion sites.

2. Model definition

Figure 1(a) shows a schematic representation of the biological system of interest. Filamentous actin (red) is polymerized at the leading edge in response to membrane-bound activators and then moves towards the cell body, where it is disassembled.

This movement is driven by the polymerization pressure at the front and by active pulling from the back by myosin II motors (green). Using fluorescent markers for the moving actin, one observes that the velocity of this backward movement strongly decreases from the cell edge towards the cell body [14]. This observation has been made in all cell types studied before and the common interpretation is that movement is slowed down by friction between the moving actin and cell adhesion contacts [10, 11]. These cell adhesions (focal adhesions, FAs) are organized around a layer of transmembrane receptors from the integrin-family (black) binding to the ligands on the substrate. On the cytoplasmic side, they couple to the moving actin cytoskeleton through a layer of adapter proteins (blue). Continuous formation and rupture of bonds between the FA and the moving actin cytoskeleton is one main mode of dissipation. However, another important mode is dissipation inside the cytoskeleton, for example by sliding friction between neighboring actin fibers as indicated by showing several parallel fibers. The localization of these two different dissipation mechanisms is indicated by the yellow boxes and corresponds to two different types of forces counteracting retrograde flow.

In figure 1(b) we depict our modeling approach to this biological system. We model the flowing actin cytoskeleton as a rigid slider which is driven over the substrate by a constant driving force F_D (right arrow). The driving force represents the combined effects of actin polymerization at the leading edge and myosin contractility at the back end of the lamellum. Alternatively one could assume a constant driving velocity. However, the assumption of constant driving velocity is not very natural because this system is dominated by force-generating processes. Here we proceed by assuming a constant driving force F_D as the main model parameter determining the instantaneous flow velocity v. In our model, it is balanced by two time-dependent forces reflecting the two main modes of dissipation considered here. The first force counteracting the driving force is the elastic force κx resulting from bonds with effective spring constant κ being continuously stretched to extension x at the moving interface (bottom left arrow). Although the bond response is elastic, the overall process is dissipative due to the continuous formation and rupture of bonds. A second counteracting force is the viscous friction force ξv arising from the immersion of the slider into the actin mesh (top left arrow). One can think of an actin fiber which has a multitude of interactions with the surrounding actin network, resulting in an overdamped dynamics with an effective viscous friction coefficient ξ. In addition, we note that the force-generating mechanisms (in particular the myosin II motors pulling at the back) also have some dissipative parts (represented e.g. by the velocity-dependent part of the effective force–velocity relation of myosin II), which also contribute to internal dissipation.

We consider a slider binding to an adhesion of constant size, thus a constant maximal number of N bonds can form. For each bond, a time-dependent occupancy variable $q_i(t) \in \{0, 1\}$ $(1 \leqslant i \leqslant N)$ describes whether a bond is open or closed. Each of these bonds is assumed to behave like a Hookean spring with spring constant κ and time-dependent extension $x_i(t)$. Our central model equation is the balance of the three forces involved:

$$F_\mathrm{D} = \xi\, v(t) + \kappa \sum_{i=1}^{N} q_i(t) x_i(t). \tag{1}$$

Note again that F_D is a constant model parameter and that in between binding and rupture events (when the q_i change), the ensemble behaves like a simple Kelvin–Voigt body. One can describe the motion of the slider iteratively by first solving equation (1) for time-dependent velocity $v(t)$ and then propagating the bond extensions, which in turn determine the new velocity. In the absence of any bond dynamics, the system would come to a halt because bond extensions would only increase and eventually the elastic bond forces would completely balance the driving force. In the presence of bond dynamics, bond rupture will relax the elastic forces and thus allow further movement of the interface. Note that the elastic bond force is the one which is measured as a local traction force at the FAs. When all bonds were open ($q_i = 0$), the slider would simply move with constant velocity $v = F_\mathrm{D}/\xi$.

For bond dynamics, we again make simple but non-trivial assumptions. For the rupture rate of single bonds we use the well-known Bell–Evans formula, $k_\mathrm{rupt}(x) = k_- \mathrm{e}^{r x_i}$ [21–23], which models bond rupture as an adiabatic escape over a sharp transition state barrier. Here the stretch x_i is assumed to correspond to the one-dimensional reaction coordinate for the detachment process. The prefactor in the exponent of the rupture rate formula is given by the reactive compliance $r = \kappa x_\mathrm{b}/k_\mathrm{B}T$, where the reaction length x_b can be identified with the distance between the bound and transition states along the reaction coordinate. We assume that binding occurs with a constant probability once a bond is open, thus we use a constant binding rate $k_\mathrm{bind} = k_+$. Each newly formed, closed bond starts with zero extension ($x_i = 0$). For a bond cluster of constant size loaded in the vertical direction by a constant and equally shared force, it has been shown before that the interplay between the non-linear rupture force and the statistics of multiple bonds leads to cooperative effects, including rupture cascades and a stability threshold under force [24]. In the case considered here, force is not shared equally, but distributed heterogeneously depending on the time point of bond formation and the velocity of the moving interface.

For our computer simulations, we make use of the next-reaction variant of the Gillespie algorithm [25]. Calculation of waiting time distributions for binding and unbinding events presupposes the usage of the solution of equation (1) to determine the evolution of each linkage in the time between two events, $x_i(t+\tau) = x_i(t) + [1 - \exp(-\kappa n \tau/\xi)][F_\mathrm{D} - \kappa \sum_j q_j(t) x_j(t)]/(\kappa n)$. Here $n = \sum_{i=1}^{N} q_i$ is the number of closed bonds at time t. The cumulative probability of each bond to survive a time τ_i is given by $\Theta(\tau_i) = 1 - \exp(-\int_t^{t+\tau_i} k_{\mathrm{rupt},i}(t', \{x_j(t)\})\,\mathrm{d}t')$. In our simulations we assign uniformly distributed random numbers Ξ_i to this probability and invert the equation to produce waiting times for all linkages, $\tau_i = \Theta^{-1}(\Xi_i)$. The event with the shortest waiting time τ_min is selected and the system is propagated

accordingly using equation (1) before the occurrence of the event. The inversion of the integral in $\Theta(t)$ can not be done analytically and we therefore resorted to the usage of precomputed lists of integrals and series expansions. This introduces slight errors which are however negligible for our purposes. The data presented below was also cross-checked with results obtained from an Euler-like algorithm employing fixed, small time steps.

3. Mean field treatment

In the following we suggest a formalism to analytically describe the model defined above and derive an approximation for the first moments of speed and friction. Let $p(x,t,q=1)$ be the probability distribution function of a bond to be bound ($q=1$) and stretched to an extent x at time t. Conversely, $\delta(x)p(t,q=0)$ denotes the probability that the bond is in the unbound state. Because we assume instantaneous relaxation after rupture, this state is always associated with $x=0$. We only deal with bond extensions $x \geqslant 0$, therefore the normalization of the delta function $\delta(x)$ is defined such that $\int_0^\infty \delta(x)\,\mathrm{d}x = 1$. We then require

$$\int_0^\infty [p(x,t,q=1)+\delta(x)p(t,q=0)]\,\mathrm{d}x = 1. \quad (2)$$

The equations governing the evolution of the probability of the bound state can be derived by considering a discretized probability distribution. The probability to be at extension x is shifted after Δt to a position $x+\Delta x$. However, during Δt there is also a decrease of probability to be bound due to possible rupture events. Conversely, binding events increase the probability to be bound and are assumed to occur only at $x=0$. The balance of influx and outflux in the small interval Δx is given by

$$\begin{aligned} &v(x+\Delta x)p(x+\Delta x,t+\Delta t,q=1)-v(x)p(x,t,q=1)\\ &\quad=\Delta x\,\{-k_{\mathrm{rupt}}(x)p(x,t,q=1)\\ &\qquad+\delta(x)[k_{\mathrm{bind}}p(t,q=0)-v(x)p(x,t,q=1)|_{x=0}]\}. \end{aligned} \quad (3)$$

The first term on the right-hand side describes rupture of bonds, the second formation of bonds with zero extension and the third represents the boundary condition that there is no influx of probability from the region $x<0$. An explicit time dependence of speed $v(t)$ is changed through equation (1) to an implicit time dependence $v(x)$ via the bond stretch $x(t)$. Expanding $p(x+\Delta x,t+\Delta t,q=1)$ and $v(x+\Delta x)$ and using $v(x)=\Delta x/\Delta t$ yields to first order a continuity equation:

$$\begin{aligned} &\partial_t p(x,t,q=1)+\partial_x\left[v(x)p(x,t,q=1)\right]\\ &\quad=-k_{\mathrm{rupt}}(x)p(x,t,q=1)+\delta(x)[k_{\mathrm{bind}}p(t,q=0)\\ &\qquad-v(x)p(x,t,q=1)|_{x=0}] \end{aligned} \quad (4)$$

with the boundary condition at $x=0$

$$0 = k_{\mathrm{bind}}p(t,q=0)-v(x)p(x,t,q=1)|_{x=0}. \quad (5)$$

The complementary equation for the evolution of the probability of the unbound state $\delta(x)p(t,q=0)$ reads

$$\begin{aligned} \delta(x)\partial_t p(t,q=0) &= \delta(x)\left[\int_0^\infty k_{\mathrm{rupt}}(x')\,p(x',t,q=1)\,\mathrm{d}x'\right.\\ &\quad\left.-k_{\mathrm{bind}}p(t,q=0)\right]. \end{aligned} \quad (6)$$

These equations conserve probability as required by equation (2). In the model introduced in the preceding section we always have $v(x)\geqslant 0$. This assumption gives rise to a jump in $p(x,t,q=1)$ at $x=0$. The introduction of the boundary term $-v(x)p(x,t,q=1)|_{x=0}$ in equation (4) is necessary to guarantee conservation of probability under these conditions. Setting $v=0$ we get the usual master equation for a two-state system. The description could also be augmented by an additional second derivative term accounting for possible noise in the system. This would lead to a form similar to the differential Chapman–Kolmogorov equation [26].

The equations for a single bond can now be generalized to an ensemble of bonds with extension $\mathbf{x}$ attached to the same fiber and thus stretched with the same speed $v(\mathbf{x})$:

$$\begin{aligned} \partial_t p(\mathbf{x},t,\mathbf{q}) &= \sum_i -\delta_{q_i,1}\partial_{x_i}[v(\mathbf{x})p(\mathbf{x},t,\mathbf{q})]\\ &\quad+\delta_{q_i,1}[-k_{\mathrm{rupt}}(x_i)p(\mathbf{x},t,\mathbf{q})+[k_{\mathrm{bind}}p(\mathbf{x},t,\mathbf{q}|q_i=0)\\ &\quad-\delta(x_i)v(\mathbf{x})p(\mathbf{x},t,\mathbf{q})|_{x_i=0}]]\\ &\quad+\delta_{q_i,0}\left[\delta(x_i)\int_0^\infty k_{\mathrm{rupt}}(x_i')\,p(\mathbf{x},t,\mathbf{q}|q_i=1)|_{x_i=x_i'}\,\mathrm{d}x_i'\right.\\ &\quad\left.-k_{\mathrm{bind}}p(\mathbf{x},t,\mathbf{q})\right] \end{aligned} \quad (7)$$

where the boundary condition is integrated, as in equation (4), into the third line on the right-hand side. The notation $\mathbf{q}|q_i=0,1$ indicates a permutation of q_i where also the corresponding x_i dependence is changed between a delta function and a continuous function. One can calculate the evolution of the probability distribution of a single bond with index k in the bound state ($q_k=1$) by summing over all the other states and integrating over their distribution of bond stretch

$$\begin{aligned} &\prod_{i\neq k}\int\sum_{\{\mathbf{q}\}}\partial_t p(\mathbf{x},t,\mathbf{q})\,\mathrm{d}x_i\\ &\quad=-\partial_{x_k}\prod_{i\neq k}\int\sum_{\{\mathbf{q}\}}[v(\mathbf{x})p(\mathbf{x},t,\mathbf{q})]\,\mathrm{d}x_i\\ &\qquad-k_{\mathrm{rupt}}(x_k)p(x_k,t,q_k=1)+\delta(x_k)\left\{k_{\mathrm{bind}}p(t,q_k=0)\right.\\ &\qquad\left.-\prod_{i\neq k}\int\sum_{\{\mathbf{q}\}}[v(\mathbf{x})p(\mathbf{x},t,\mathbf{q})|_{x_k=0}]\,\mathrm{d}x_i\right\}. \end{aligned} \quad (8)$$

The remaining equation for the unbound state ($q_k=0$) corresponds to equation (6). This equation illustrates that coupling of the bond states is only mediated by the common speed $v(\mathbf{x})$ which appears in the integrals on the right-hand side. Given that $v(\mathbf{x})$ depends on the stretch of all bonds, these integrals are the expectation value of $v(\mathbf{x})$ under the condition that bond k has stretch x_k. In a mean field ansatz we write here

$$\prod_{i\neq k}\int\sum_{\{\mathbf{q}\}}q_k v(\mathbf{x})\,p(\mathbf{x},t,\mathbf{q})\,\mathrm{d}x_i \approx \langle v\rangle\,p(x_k,t,q_k=1). \quad (9)$$

Using this approximation in equation (8) the probability distributions of different bonds factorize. We thus recover the equation for a single bond, equation (4), where we now replace $v(\mathbf{x})$ with an average speed $\langle v\rangle$ which needs to be determined separately. This approximation is expected to work well if

the number of bound bonds is high, so that the effect of one single bond does not significantly change the velocity. We also introduce a mean field equation of motion, which we use together with equation (9) for an approximation of $\langle v\rangle$:

$$\langle v\rangle = \frac{F_{\mathrm{D}}}{\xi} - \frac{N f(\langle v\rangle)}{\xi}, \tag{10}$$

where $f(\langle v\rangle)$ is the average force transmitted by each linker. Equations (2), (4), (5) and (6) can be solved for the steady state:

$$p(x, q=1) = \frac{p(q=0) k_+ e^{\epsilon_- (1-\mathrm{e}^{rx})}}{\langle v\rangle} \tag{11}$$

$$p(q=0) = \frac{1}{1+\epsilon_+ e^{\epsilon_-} \Gamma_{\epsilon_-}(0)} \tag{12}$$

with $\epsilon_- = k_-/r\langle v\rangle$ and $\epsilon_+ = k_+/r\langle v\rangle$. Thus while unbound bonds only exist with extension $x = 0$, the distribution of the extension x for the bound bonds decays faster than exponential from $x = 0$ to positive values of x. The average force transmitted by each linker can be calculated from the expectation value of the stretch:

$$\begin{aligned} f(\langle v\rangle) &= \kappa \int_0^\infty x p(x, q=1)\,\mathrm{d}x \\ &= \kappa \frac{p(q=0)\, k_+}{\langle v\rangle} \int_0^\infty x e^{\epsilon_- (1-\mathrm{e}^{rx})}\,\mathrm{d}x, \end{aligned} \tag{13}$$

where the last integral could also be formally expressed as a Meijer function. For high average speeds the transmitted force becomes zero: $\lim_{\langle v\rangle\to\infty}[f(\langle v\rangle)] = 0$. For large ϵ_- (fast unbinding), one can perform asymptotic expansions of the integral in equation (13) and the Gamma function in equation (12). This leads to:

$$\begin{aligned} f(\langle v\rangle)_{\mathrm{weak}} &= \frac{k_+}{(k_- + k_+)} \frac{\kappa\langle v\rangle}{k_-}, \\ p(q=0)_{\mathrm{weak}} &= \frac{k_-}{(k_- + k_+)}. \end{aligned} \tag{14}$$

In this regime, the average friction force is simply the spring constant κ times the typical extension $\langle v\rangle/k_-$ times the mean number of closed bonds.

4. Estimation of parameters

In the following we give order-of-magnitude estimates for the different model parameters in order to compare our theoretical results to experimental data. A typical extension of an adhesion site in the direction of flow is 1 μm, while the perpendicular extension is considerably smaller. With a typical adhesion protein spacing of 30 nm we estimate the ligand number to be $10 \lessapprox N \lessapprox 1000$. Mechanical connections between the actin cytoskeleton and the substrate involve a hierarchy of different bonds, including those mediated by adapter proteins such as talin as well as the integrin–matrix bonds. Experiments have shown that the linkage between integrins and their extracellular ligands is quite strong [27, 28], whereas the intracellular bond to actin is relatively weak [29]. Therefore, one expects that the linkage between the cytoskeleton and the extracellular side predominantly breaks at one site, for example the connection between actin and talin. However, the effective spring constant of the bond will depend on the contributions of all the different proteins and the elastic environment. These can only be inferred indirectly. AFM measurements report overall cell stiffnesses of 0.01–5 pN nm^{-1} [30, 31]. We expect that the contribution of elasticity of the ECM and intracellular effects on small length scales will give a somewhat larger spring constant of around $\kappa = 10$ pN nm^{-1}. Typical reaction lengths x_{b} of adhesion bonds are about 0.2 nm [31], thus setting r to about 0.5 nm^{-1}. The force-free unbinding rate k_- is, for most biological adhesion bonds, on the scale of 1 s^{-1} and we will hence use this value.

Concerning the binding rate k_+ the situation is much more complex. Binding constants can only be inferred from a few known affinity measurements. Equilibrium (bulk) association constants for the binding of talin-like proteins to integrins or to actin are known to be in the range of 10^6–10^7 M^{-1} (1 M^{-1} $\approx$ 1.7 nm^3) [32–34]. Integrins have at least two different activity states in which their binding rates are very different. Evidence for this is that the binding affinity of integrins to extracellular matrix ligands in the inactive state is reported to be $<10^6$ M^{-1}, while it increases more than ten fold in the active state [35–37]. Interestingly, the unbinding rate seems to change relatively little with activation of integrins. The existence of this affinity switch suggests that the process of linkage formation between actin and the extracellular ligands is largely limited by integrin binding in the inactive state, while intracellular bond formation is limiting in the active state.

Application of the above values to the FA structure is impeded by the fact that spatial confinement of FA proteins to the two-dimensional adhesion structure modifies diffusion and thus also the affinity. Due to experimental difficulties there are to date not many reliable measurements of this effect. Simple theoretical estimates suggest that a factor of $1/\vartheta \approx 1/20$ nm is appropriate for the conversion of the three-dimensional association constant to its two-dimensional counterpart [21]. However, experiments showed that this factor is much lower, which is possibly due to a reduced accessibility of binding sites in two dimensions [38, 39]. Here we accordingly use $1/\vartheta \approx 10^{-4}$ nm. We estimate the number of binding events per second with the following formula: $k_+ \approx K_{\mathrm{bulk}} \times k_- \times 1/\vartheta \times \Phi_b$. Using $k_- \approx$ s^{-1} and linker density $\Phi_b \approx 2\times10^{-4}$–$10^{-3}$ nm^{-2} [40] we find for the inactive ligand complex 10^6 nm^3 s^{-1} $\cdot$ 10^{-4} nm^{-1} $\cdot$ $\Phi_b \approx$ 0.02–0.1 s^{-1}. The binding rate for active integrins can accordingly be expected to be above 1/s, which may also be necessary to permit growth of the adhesion structure which dissociates with an unbinding rate of $k_- \approx$ s^{-1}.

The internal viscous friction coefficient ξ summarizes many different effects and is therefore not easy to estimate. Its units are viscosity $\times$ length and in a hydrodynamic picture it would be the drag coefficient of a slender fiber. A rough estimate of the viscous friction coefficient can be based on the observation that in the lamellipodium of migrating cells, we hardly have any adhesion sites and the actin velocity ranges up to 100 nm s^{-1} [14]. Corresponding polymerization/membrane forces are about $F_{\mathrm{D}} \approx$ 5–100 pN. This implies that ξ is on

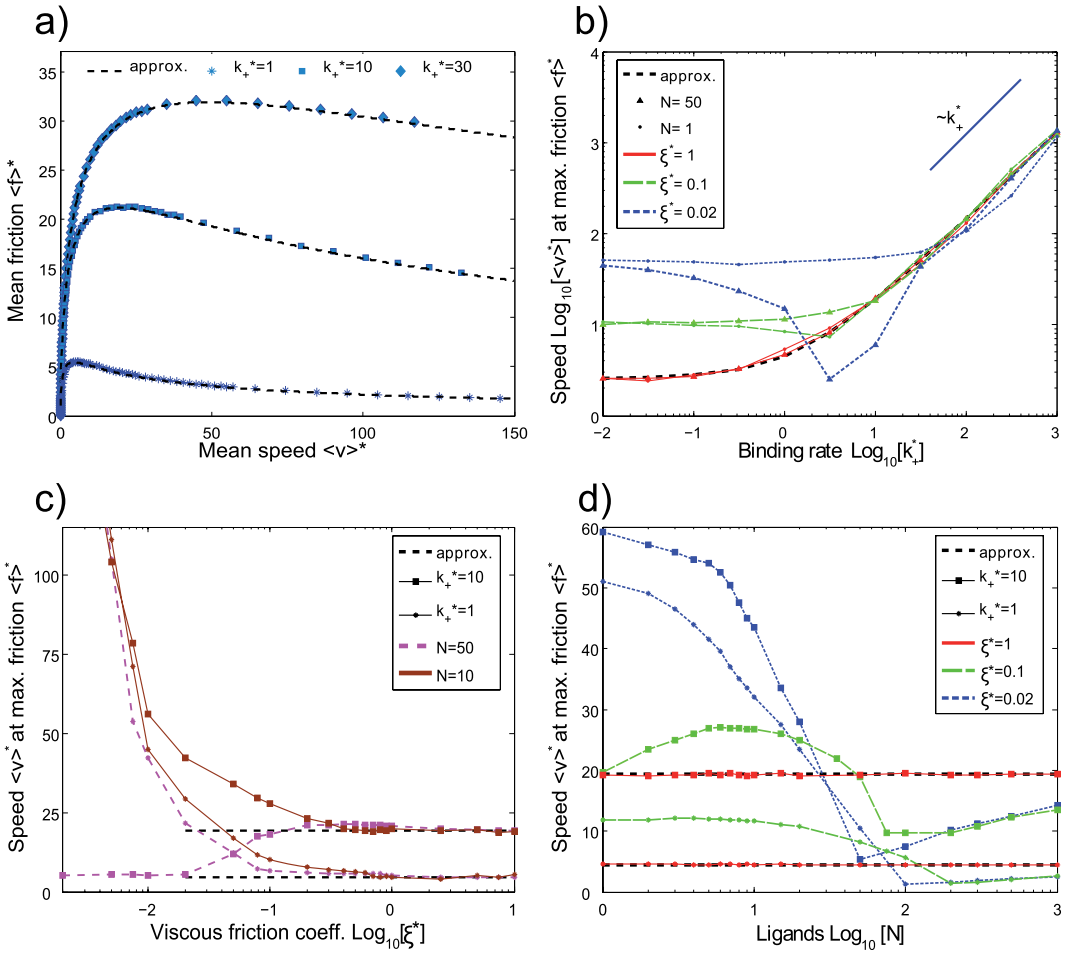

Figure 2. Biphasic relationship between dimensionless mean speed and mean friction. (a) First moments of friction and speed obtained from simulation ($N = 25, \xi^* = 1$) and the corresponding mean field approximations. (b) Average speed at maximal average friction depends almost linearly on binding rate. (c) Average speed at maximal average friction becomes independent of ξ^* and N for high viscous friction. (d) Average speed at maximal average friction strongly depends on N for low ξ^*.

the order of 1 pN s nm^{-1} but will vary strongly depending on how crosslinked the actin meshwork is [3]. In particular, it is expected to be higher in the lamellum (where it flows over the adhesions) than in the lamellipodium (where hardly any adhesions exist). This estimate can be compared to published values of the effective long-timescale viscosity in the actin cortex when converting the viscosity to a hydrodynamic drag coefficient of a slender fiber using typical length scales of the fiber (length 2 μm, width 1 nm). For a viscosity of 300 Pa s (see e.g. [41, 42]) the drag coefficient is about 0.6 pN s nm^{-1}, which agrees reasonably well with our estimate from the experimental data.

In summary, our model parameters are driving force F_D, ligand number N, internal viscous friction coefficient ξ, bond stiffness κ, unstressed unbinding rate k_-, binding rate k_+ and reactive compliance r. In the following we will rescale time with the unstressed unbinding rate k_-, length with the inverse reactive compliance $1/r$ and force with κ/r. Reference values for driving force F_D, velocity v and internal viscous friction coefficient ξ are therefore 20 pN, 2 nm s^{-1} and 10 pN s nm^{-1}, respectively. Dimensionless quantities are indicated by an asterisk. For example, for a typical actin speed of $v = 10$ nm s^{-1} we have $v^* = v\,r/k_- = 5$. The above estimate for internal friction in the lamellipodium gives $\xi^* = 0.1$. This value is expected to increase in the lamellum, where retrograde flow couples to the adhesions.

5. Results

Figure 2(a) displays the average elastic friction (traction) force $\langle f \rangle^*$ transmitted at an average speed $\langle v \rangle^*$ as obtained from the computer simulations of the full model ($N = 25, \xi^* = 1$). Parameters in the simulation were chosen here such that a good correspondence between the mean field model and simulations could be demonstrated. The relation between average friction and speed is always distinguished by a maximum in friction at intermediate speeds which can also be found analytically from the mean field approximation. The occurrence of this maximum can be explained in the framework of the mean field model by the fact that the average transmitted force at a closed bond rises monotonously with speed, while the probability of being bound decreases at higher speed. The combination of both factors produces the characteristic shape

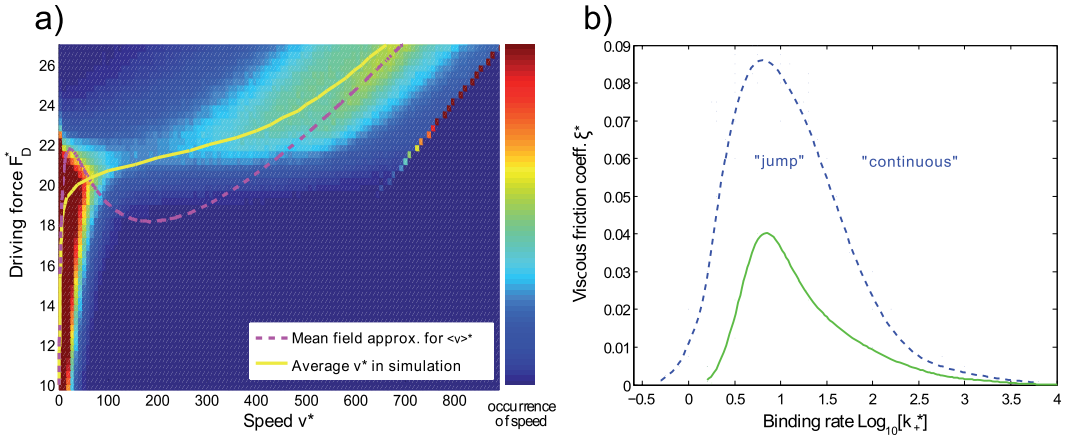

Figure 3. Transition regime at intermediate driving forces. (a) Color-coded probability distribution for speed in numerical simulations and first moment of speed in simulation and mean field approximation ($N = 25, \xi^* = 0.03, k_+^* = 10$). Irregular motion with large fluctuations occurs at intermediate driving forces and is characterized by a broad, multi-modal probability distribution. (b) Parameter dependence of the occurrence of a regime with strong speed fluctuations as shown in (a). This occurrence was determined numerically through the strong sensitivity of the transmitted friction force $\langle f \rangle^*$ on the (constant) driving force F_D^* in the critical regime. Dotted line for $N = 50$, full line for $N = 25$.

seen in figure 2(a), with average friction increasing much more strongly at low $\langle v \rangle^*$ than decaying at high speed.

The maximum in the friction–speed plot offers a convenient way to characterize the behavior of the simulated model and to compare it with the mean field approximation. In figure 2(b) we plot the binding rate dependence of $\langle v \rangle^*$ at maximum average friction $\langle f \rangle^*$. If the timescale of binding is much shorter than the timescale of viscous relaxation, $1/k_+ \ll \xi/\kappa$, one expects a good transmission of force because fast rebinding weakens cooperative effects. Indeed, here the results from simulations agree well with the analytical approximation. Within the mean field model it can be shown that the relationship between binding rate k_+^* and speed $\langle v \rangle^*$ at maximum friction obeys the following asymptotic relation for high binding rates:

$$k_+^* \approx \left(1 + 2\frac{6(\gamma_e - \ln\langle v\rangle^*) + \pi^2}{6(\gamma_e - \ln\langle v\rangle^*)^2 - \pi^2}\right)\langle v\rangle^* - 1, \qquad (15)$$

where γ_e is the Euler–Mascheroni constant. The linear relation can be clearly observed in the simulation results for large k_+^*. For the limit $k_+^* \to 0$ the location of maximal $\langle f \rangle^*$ converges in the mean field model to a constant $\langle v \rangle^* \approx 2.568$. This mean field behavior at low binding rates is in contrast to the simulation results, where the dependence of speed at maximum friction depends on ξ^* and N. However, the mean field model can also be recovered in the simulations for low k_+^* when the viscous friction coefficient is high, $1 \lessapprox \xi^*$. Therefore we plot in figure 2(c) the dependence of $\langle v \rangle^*$ at maximum average friction on the viscous friction coefficient ξ^*. If $1 \lessapprox \xi^*$ (meaning that the timescale of viscous relaxation is longer than the timescale of unbinding) one generally sees a good correspondence between mean field model and simulations. In the mean field approximation, the location of maximal friction does not depend on ξ^*. For lower values of ξ^*, the average speed at maximum friction shows an interesting behavior which results from irregular slip and stick motion which we will discuss below.

Figure 2(d) shows the dependence of average speed $\langle v \rangle^*$ at maximum average friction on the number of linkage molecules N. In the mean field approximation, the transmitted elastic friction is simply linear in N. We consider whether a high number of ligands N is sufficient to reproduce this mean field behavior in our simulations at $\xi^* < 1$. As can be seen from figure 2(d), the simulation results approach the mean field solution for large N, but one would need $N \gtrapprox 10^4$ to obtain a reasonable agreement between both. The required numbers of ligands are beyond what we would expect for the biological system in question (see section 4). We conclude that cooperative effects are suppressed in our model less efficiently by a high number of ligands than by a high viscous friction coefficient.

In summary, the mean field description breaks down for $\xi^* < 1$. This is also reflected by the fact that the location of maximum friction at low ξ^* in figures 2(b)–(d) shows a non-monotonous behavior. To investigate this in detail we color code in figure 3(a) the probability distribution for the occurrence of speed in a numerical simulation ($N = 25, \xi^* = 0.03, k_+^* = 10$). As always, the constant driving force F_D^* is fixed. Here this independent variable is located on the y-axis. For the comparatively low viscous friction coefficient used in this simulation, the distribution of speeds displays an interesting multi-modal appearance. The figure demonstrates that for low F_D^* the system is dominated by the elastic contribution of the bonds and one has slow creep motion. For intermediate F_D^* around a value of 20, the fiber occasionally detaches and the amplitude of speed fluctuations increases. It is here that the distribution of speeds shows two or even three pronounced maxima. The fluctuations and the multi-modal appearance of the speed distribution are reminiscent of a phase transition. At high driving force the motion is dominated by the viscous friction and the contribution of the bonds can not arrest the fiber anymore.

We can again employ our analytic mean field approximation to qualitatively explain the simulation results. Within this

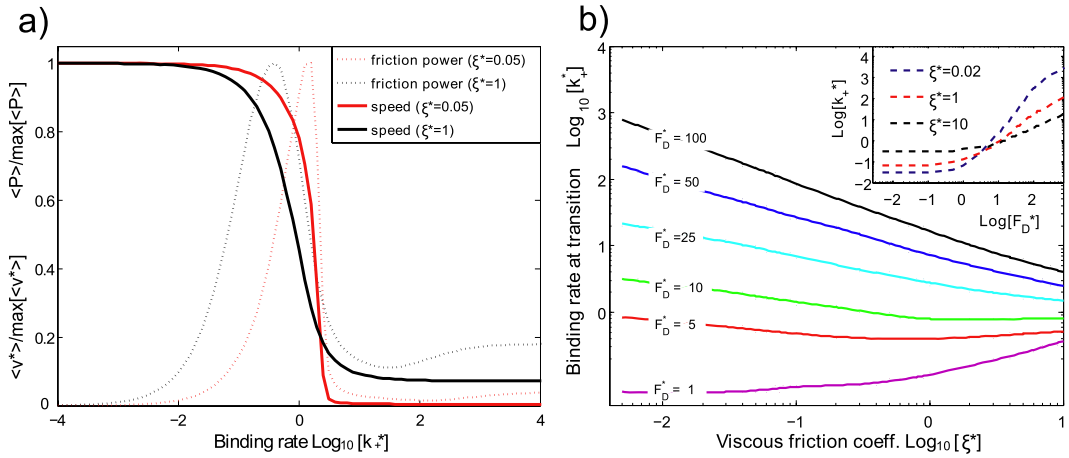

Figure 4. Active change of the binding rate enables cells to switch from viscous dissipation to elastic force transmission. (a) Relative change of average speed and average elastic friction power with varying binding rate ($F_D^* = 10$, $N = 25$). Most elastic power in the bonds is dissipated in the transition region. (b) Dependence of the transition point between high and low speed (half maximum) on various model parameters.

approximation, the driving force F_D can be expressed through the mean field equation of motion equation (10) as a function of $\langle v \rangle$. While viscous friction is linear in $\langle v \rangle$, the elastic friction shows a biphasic dependence on speed. Both contributions together result in a bistable regime where one has multiple solutions for the speed $\langle v \rangle$ at a given constant value for the driving force F_D (violet line, figure 3(a)). Note that this plot does not show the biphasic elastic friction, which decays with increasing $\langle v \rangle$. To assess how the onset of this transition depends on the model parameters, we search in our analytic approximation (where F_D is written as a function of $\langle v \rangle$) for a saddle point. Critical points in the k_+–ξ plane are then given by $\partial_{\langle v \rangle} F_D = \partial^2_{\langle v \rangle} F_D = 0$. Qualitatively, we find that a discontinuous transition between different speeds occurs only for intermediate values of k_+^*. This is so because the system is dominated at low k_+^* by the viscous friction, and rare binding of bonds can not arrest the fiber. High k_+^*, on the other hand, prevents a sudden detachment of the fiber, and hence also damps speed jumps. The value of ξ^* below which we can have discontinuous speed changes increases in the mean field linearly with N. Thus, increasing the ligand number and driving force without changing ξ promotes the occurrence of an unstable regime with large speed fluctuations.

A direct comparison of the picture suggested by the mean field model with the results from stochastic simulations is impeded by the lack of a clear analog to the critical point in the simulations. However, in a certain range of parameters we observe a strong change in $\langle f \rangle^*$ if the (constant) driving forces F_D^* are changed only slightly between different runs of the simulation. This sudden change happens e.g. in figure 3(a) at intermediate F_D^* and is accompanied by strongly fluctuating speed values. Our numerical criterion for the occurrence of a quasi-discontinuous transition with strongly fluctuating speeds was here that $\partial_{F_D^*} \langle f^*(F_D^*) \rangle \leqslant -5.5$ for any (constant) value of F_D^* at fixed k_+^* and ξ^*. The results are plotted in figure 3(b) for two values of N. Qualitatively, the approximate state diagram shows the same shape as the lines of critical points explained above for the mean field approximation.

Regarding the biological system of interest, the binding rate k_+ constitutes the regulatory parameter which is most likely to be actively changed by the cell. For very low binding rates, internal friction dominates the motion, while for high binding rates the elastic friction dictates a creep motion. Figure 4(a) depicts the corresponding transition for two values of the viscous friction coefficient ($F_D^* = 10, N = 25$). The transition from the viscous regime at high speed to the elastic regime occurs within a zone of 10–100 fold change in the binding rate. Lowering the viscous friction leads to an increased maximal slope of the curve, which again results in the mean field approximation in a discontinuity. A comparison of the analytical approximation and simulations showed that the analytical description, in general, works better in the low speed elastic regime. Plotting the dependence of bound linkages on k_+^* results in a curve which is complementary to the curve for $\langle v \rangle^*$ in figure 4(a) (not shown). However the transition from low to high fractions of bound linkages occurs at slightly different values of k_+^*.

Energy dissipation due to elastic friction at the adhesion is quantified by the friction power $\langle P \rangle = \langle v \cdot \kappa \sum q_i x_i \rangle$. It shows a peak at the transition from low to high speed where the relative height of the peak in friction power decreases with increasing viscous friction coefficient, compare figure 4(a). The binding rate at which the transition from the viscous to the elastic regime occurs depends on all free parameters in our system. In figure 4(b) we plot this dependence for $N = 25$. While the binding rate at the transition can increase or decrease with ξ^*, depending on F_D^*, an increasing driving force always leads to a shift of the transition to higher binding rates (see inset). For a number of ligands $N \gtrapprox 10$ the binding rate at the transition scales approximately as $1/N$ (data not shown). Summarizing, we find that a 10–100 fold change of the binding rate is the appropriate range to control whether the fiber is in the elastic creep regime, where dissipation of energy is small, or in the viscous regime, where most of the power is dissipated to the surrounding viscous medium.

6. Discussion

Motivated by recent experiments on the transmission of force from the flowing actin cytoskeleton to the cell substrate [14], the main focus of this work was to investigate in a simple theoretical model how dynamical bonds transmit force through a moving interface. Related models have been studied in the past in the context of tribology [16–18], but here we study this question with a special focus on the cellular system. Adhesion sites are modeled as collections of dynamically binding and unbinding bonds forming elastic connections to a rigid slider which is dragged through a viscous intracellular environment by a constant driving force. Our model results in surprisingly rich behavior, including a biphasic friction law and a stick–slip regime, which both appear to be highly relevant for the biological system of interest. Due to its simplicity, the model introduced here can be used as a reference and starting point for more realistic descriptions of the dynamics of force-bearing elements in biological systems.

Experimental results demonstrating a maximum in cellular traction at local actin speed around 10 nm s^{-1} [14] leave room for a number of interpretations. The finding is closely related to the spatial distribution of adhesion molecules but relatively independent of biochemical perturbations such as interference with the small GTPases Rho and Rac. Therefore, here we focused on generic effects resulting from sliding friction at moving interfaces. In setting up the model, we made some crucial assumptions which are motivated by the biological system of interest. First, we have summarized all dissipative processes, including actin polymerization at the leading edge, crosslinker dynamics in the gel, and molecular motor activity at the back, by an effective viscous friction coefficient ξ. In the future, one can envision introducing more detailed modeling of the material properties of the actin gel, in particular dynamic rearrangements within the gel [43]. Another core assumption of the presented model is the presence of a constant driving force F_D. Here more detailed models for actin polymerization and force generation by molecular motors are possible, for example as used recently for modeling filopodia retraction [19]. Note that introducing an internal viscous friction coefficient ξ can also be interpreted as arising from a linear force–velocity relation for the molecular motors driving the flow.

To qualitatively understand our simulation results we use a mean field model where not only the driving force F_D is constant but where speed $v(t)$ equals a constant $\langle v \rangle$ for all times. This limit corresponds to a constant speed ensemble where the bond states do not couple via equation (1) because rupture does not entail an acceleration of the slider. Within the framework of our stochastic model, we find that high internal friction $\xi^* \gtrapprox 1$ diminishes the role of cooperativity and thus allows for a mean field description. This then implies that the speed $\langle v \rangle$ at which the transmitted friction $\langle f \rangle$ is maximal depends neither on the number of bonds N nor on the exact value for the effective viscosity. The value of the transmitted friction force simply scales with the number of linkage molecules.

In the limit of high viscous friction coefficient $\xi^* \gtrapprox 1$ the dimensionless binding rate k_+^* dominates the system. The speed at maximal friction $\langle f \rangle^*$ is a unique function of this parameter. The maximum in $\langle f \rangle^*$ can possibly be observed in experiments. This could provide a way to estimate properties of adhesion proteins which are otherwise hard to assess. For example, if one assumes that one can apply this reasoning to the experimental data in [14], then a speed at maximum traction of 10 nm s^{-1} with $r = 0.5$ nm^{-1} would lead to $k_+/k_- \approx 1.3$.

For a small viscous friction coefficient, the mean field description of our system fails. When the timescale of viscous relaxation becomes smaller than the timescale of bond rupture, $\xi/\kappa < 1/k_-$ (and not $\xi/\kappa \gg 1/k_+$), the probability distribution for the bond states can no longer be approximated by a factorized distribution. Then the mean field equation of motion (10) becomes inappropriate. Here the rupture of one bond can trigger rupture cascades similar to ones described before [24]. Motion at low ξ accordingly consists of alternating phases of stick and slip. The viscous friction coefficient below which we find this strongly irregular motion increases with the number of bonds. Thus a moderate increase in the number of ligands is not necessarily sufficient to stabilize adhesion against forces. The rupture cascades and irregular motion patterns found in our model are reminiscent of the motion of actin in the lamellipodium, as observed in experimental data [14].

It is interesting to note that the intermediate region between elasticity-dominated creep and viscosity-dominated flow is special for energetic reasons. Although the averaged power dissipated by the cellular machinery is, in our model, proportional to the average speed, one can ask whether the power is spent efficiently. In the transition zone between high and low flow speeds much power is invested in friction with the substrate while both the transmitted force and the speed of the fiber are comparatively low. Accordingly, neither transport nor force transmission can be accomplished efficiently in this regime.

In summary, we have proposed a simple model to assess how the dynamics of individual bond formation and rupture could translate into a non-linear relationship between mean values of friction and speed at adhesion sites, and how the binding processes at the moving interface compete with dissipation inside the cell. In the future our simulations could be extended in many directions to accommodate more detailed modeling of such cellular systems. In particular, it would be most interesting to replace the effective internal viscous friction coefficient used here by more microscopic models for competing binding processes, thus modeling both dissipation mechanisms on an equal basis.

Acknowledgments

The authors thank Margaret Gardel, Sergej Plotnikov, Clare Waterman and Christian Korn for helpful discussions. BS especially thanks Hyoung Ju Song for her loving support. This work was supported by the Center for Modeling and Simulation in the Biosciences (BIOMS) and the Cluster of Excellence CellNetworks at Heidelberg.

References

[1] Geiger B, Spatz J P and Bershadsky A 2009 Environmental sensing through focal adhesions *Nat. Rev. Mol. Cell Biol.* **10** 21–33

[2] Lauffenburger D A and Horwitz A F 1996 Cell migration *Cell* **84** 359–69

[3] Besser A and Schwarz U S 2007 Coupling biochemistry and mechanics in cell adhesion: a model for inhomogeneous stress fiber contraction *New J. Phys.* **9** 425

[4] Theriot J A and Mitchison T J 1991 Actin microfilament dynamics in locomoting cells *Nature* **352** 126–31

[5] Hotulainen P and Lappalainen P 2006 Stress fibers are generated by two distinct actin assembly mechanisms in motile cells *J. Cell Biol.* **173** 383–94

[6] Mitchison T and Kirschner M 1988 Cytoskeletal dynamics and nerve growth *Neuron* **1** 761–72

[7] Lin C H and Forscher P 1995 Growth cone advance is inversely proportional to retrograde F-actin flow *Neuron* **14** 763–71

[8] Jurado C, Haserick J R and Lee J 2005 Slipping or gripping? Fluorescent speckle microscopy in fish keratocytes reveals two different mechanisms for generating a retrograde flow of actin *Mol. Biol. Cell* **16** 507–18

[9] Guo W H and Wang Y L 2007 Retrograde fluxes of focal adhesion proteins in response to cell migration and mechanical signals *Mol. Biol. Cell* **18** 4519–27

[10] Wang Y L 2007 Flux at focal adhesions: slippage clutch, mechanical gauge, or signal depot *Sci. STKE* **2007** 1–3

[11] Giannone G, Mege R M and Thoumine O 2009 Multi-level molecular clutches in motile cell processes *Trends Cell Biol.* **19** 475–86

[12] Brown C M, Hebert B, Kolin D L, Zareno J, Whitmore L, Horwitz A R and Wiseman P W 2006 Probing the integrin-actin linkage using high-resolution protein velocity mapping *J. Cell Sci.* **119** 5204–14

[13] Hu K, Ji L, Applegate K T, Danuser G and Waterman-Storer C M 2007 Differential transmission of actin motion within focal adhesions *Science* **315** 111–5

[14] Gardel M L, Sabass B, Ji L, Danuser G, Schwarz U S and Waterman C M 2008 Traction stress in focal adhesions correlates biphasically with actin retrograde flow speed *J. Cell Biol.* **183** 999–1005

[15] Persson B N J (ed) 2000 *Sliding Friction: Physical Principles and Applications* (*Springer Series in Nanoscience and Technology*) (Berlin: Springer)

[16] Schallamach A 1963 A theory of dynamic rubber friction *Wear* **6** 375–82

[17] Filippov A E, Klafter J and Urbakh M 2004 Friction through dynamical formation and rupture of molecular bonds *Phys. Rev. Lett.* **92** 135503

[18] Srinivasan M and Walcott S 2009 Binding site models for friction due to the formation and rupture of bonds: state-function formalism, force–velocity relations, response to slip velocity transients, and slip stability *Phys. Rev.* E **80** 046124

[19] Chan C E and Odde D J 2008 Traction dynamics of filopodia on compliant substrates *Science* **322** 1687

[20] Macdonald A, Horwitz A R and Lauffenburger D A 2008 Kinetic model for lamellipodal actin-integrin 'clutch' dynamics *Cell Adhes. Migr.* **2** 95–105

[21] Bell G I 1978 Models for the specific adhesion of cells to cells *Science* **200** 618–27

[22] Evans E and Ritchie K 1997 Dynamic strength of molecular adhesion bonds *Biophys. J.* **72** 1541–55

[23] Shillcock J and Seifert U 1998 Escape from a metastable well under a time-ramped force *Phys. Rev.* E **57** 7301–4

[24] Erdmann T and Schwarz U S 2004 Stability of adhesion clusters under constant force *Phys. Rev. Lett.* **92** 108102

[25] Gillespie D T *et al* 1977 Exact stochastic simulation of coupled chemical reactions *J. Phys. Chem.* **81** 2340–61

[26] Gardiner C W 2004 *Handbook of Stochastic Methods for Physics, Chemistry, and the Natural Sciences* (New York: Springer)

[27] Sun Z, Martinez-Lemus L A, Trache A, Trzeciakowski J P, Davis G E, Pohl U and Meininger G A 2005 Mechanical properties of the interaction between fibronectin and $\alpha_5\beta_1$-integrin on vascular smooth muscle cells studied using atomic force microscopy *Am. J. Physiol.—Heart Circulatory Physiol.* **289** 2526–35

[28] Boettiger D, Lynch L, Blystone S and Huber F 2001 Distinct ligand-binding modes for integrin $\alpha v\beta_3$-mediated adhesion to fibronectin versus vitronectin *J. Biol. Chem.* **276** 31684–90

[29] Jiang G, Giannone G, Critchley D R and Fukumoto E 2003 Two-piconewton slip bond between fibronectin and the cytoskeleton depends on talin *Nature* **424** 334–7

[30] Pierrat S, Brochard-Wyart F and Nassoy P 2004 Enforced detachment of red blood cells adhering to surfaces: statics and dynamics *Biophys. J.* **87** 2855–69

[31] Li F, Redick S D, Erickson H P and Moy V T 2003 Force measurements of the $\alpha_5\beta_1$ integrin-fibronectin interaction *Biophys. J.* **84** 1252–62

[32] Horwitz A, Duggan K, Buck C, Beckerle M C and Burridge K 1986 Interaction of plasma membrane fibronectin receptor with talin-a transmembrane linkage *Nature* **320** 531–3

[33] Kaufmann S, Kas J, Goldmane W H, Sackmann E and Isenberg G 1992 Talin anchors and nucleates actin filaments: a direct demonstration *FEBS Lett.* **314** 203–5

[34] Meyer R K 1990 Bundling of actin filaments by alpha-actinin depends on its molecular length *J. Cell Biol.* **110** 2013–24

[35] Faull R J 1993 Affinity modulation of integrin $\alpha_5\beta_1$: regulation of the functional response by soluble fibronectin *J. Cell Biol.* **121** 155–62

[36] Suehiro K, Gailit J and Plow E F 1997 Fibrinogen is a ligand for integrin $\alpha_5\beta_1$ on endothelial cells *J. Biol. Chem.* **272** 5360

[37] Pampori N, Hato T, Stupack D G, Aidoudi S, Cheresh D A, Nemerow G R and Shattil S J 1999 Mechanisms and consequences of affinity modulation of integrin $\alpha v\beta_3$ detected with a novel patch-engineered monovalent ligand *J. Biol. Chem.* **274** 21609–16

[38] Kuo S C and Lauffenburger D A 1993 Relationship between receptor/ligand binding affinity and adhesion strength *Biophys. J.* **65** 2191–200

[39] Moy V T, Jiao Y, Hillmann T, Lehmann H and Sano T 1999 Adhesion energy of receptor-mediated interaction measured by elastic deformation *Biophys. J.* **76** 1632–8

[40] Wiseman P W, Brown C M, Webb D J, Hebert B, Johnson N L, Squier J A, Ellisman M H and Horwitz A F 2004 Spatial mapping of integrin interactions and dynamics during cell migration by image correlation microscopy *J. Cell Sci.* **117** 5521–34

[41] Lang T, Wacker I, Wunderlich I, Rohrbach A, Giese G, Soldati T and Almers W 2000 Role of actin cortex in the subplasmalemmal transport of secretory granules in PC-12 cells *Biophys. J.* **78** 2863–77

[42] Cuvelier D, Théry M, Chu Y S, Dufour S, Thiéry J P, Bornens M, Nassoy P and Mahadevan L 2007 The universal dynamics of cell spreading *Curr. Biol.* **17** 694–9

[43] Ji L, Lim J and Danuser G 2008 Fluctuations of intracellular forces during cell protrusion *Nat. Cell Biol.* **10** 1393–400